MULTISCALE SIMULATION OF THE COMPETITION BETWEEN INTERGRANULAR AND TRANSGRANULAR FRACTURE IN 7000 ALLOYS

F. Scheyvaerts[1], P.R. Onck[2] and Y. Bréchet[3], T. Pardoen[1]

[1]Département des Sciences des Matériaux et des Procédés, Université catholique de Louvain, IMAP, Place Sainte Barbe 2, B-1348, Louvain-la-Neuve, Belgium ; scheyvaerts@pcim.ucl.ac.be and pardoen@pcim.ucl.ac.be
[2] Department of Applied Physics, University of Groningen, Micromechanics of Materials, Nijenborgh 4, 9747 AG Groningen, The Netherlands ; p.r.onck@phys.rug.nl
[3] Laboratoire de Thermodynamique et Physico-chimie Métallurgiques, ENSEEG, Institut National Polytechnique de Grenoble 1130, Rue de la Piscine - Domaine Universitaire B.P. 75 F-38402 Saint Martin d'Heres cedex France ; ybrechet@ltpcm.inpg.fr

Abstract

The competition between intergranular and transgranular fracture in aluminium alloys with precipitate free zones (PFZs) along grain boundaries is investigated using a multiscale approach. Ductile fracture both in the grains and in the soft PFZ occurs through the nucleation of voids at second phase inclusions, their growth and subsequent coalescence. A grain level unit cell model has been developed in order to capture the link between the microstructure, the flow properties and the ductility, which is very much dictated by the inter- vs. trans-granular mode of cracking. The constitutive description used in both regions is an extension of the Gurson model, accounting for void shape effects, void rotation and hardening. The focus of the present paper is on the effect of the yield stress mismatch between both zones. For a high yield stress in the interior of the grains, the fracture is purely intergranular; for a low grain yield stress, the fracture is purely transgranular; and for intermediate yield stress, part of the fracture is intergranular and part of the fracture is transgranular.

1. Introduction

In some materials, spatial heterogeneities in mechanical properties and microstructural features are responsible for the coexistence of different ductile failure modes. In particular, in some aluminium alloys, the microstructure consists of precipitate free zone along the gain boundary with large second phase inclusions, and a precipitation hardened state within the grain. The failure mode of the material can be either intragranular or intergranular ductile fracture, or a combination of the two, see [1,2,3].

A schematic of the microstructure is shown in Fig. 1a. The individual features controlling the fracture of aluminium alloys are well identified. They indicate the relevant parameters to be introduced in our micromechanical model. The influence of the heat treatments will be lumped into an evolution of the yield stress and work hardening. The grain interior after heat treatment will have a high yield stress σ_{0g} and a low work hardening rate n_g. On the other hand, the PFZ will have a low yield stress σ_{0p} and a high work hardening rate n_p. The idealised microstructure is shown in Fig. 1b. The various length scales entering the problem

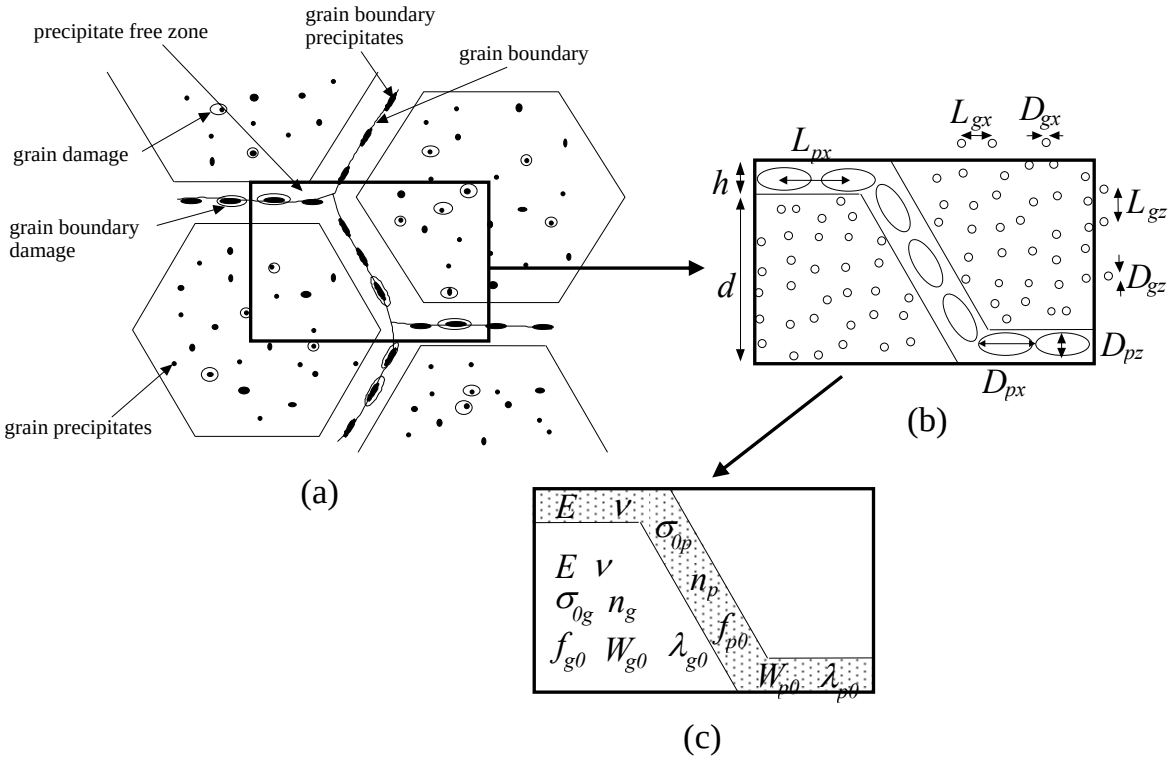

FIGURE 1. Description of (a) the real microstructure and failure mechanisms, of (b) the idealised microstructure and of (c) the continuum micromechanical model. The parameters appearing in (b) and (c) are defined in Table 1.

and the relevant dimensionless quantities which will appear in the model are given in Table 1 (The subscript (i) stands for either "p", i.e. precipitate free zone (PFZ) or "g", i.e. grain interior. A subscript "0" will be added when referring to the initial state). The density and initial size of the cavities will be considered uniform inside the grain and the PFZ. The uniaxial elastic/plastic tensile behaviour of the matrix material in the grain interior and the PFZ is described by a simple two-parameter description for the matrix stress σ_M and strain ε_M:

$$\frac{\sigma_M}{\sigma_0} = \frac{E\varepsilon_M}{\sigma_0} \quad \text{when } \sigma_M < \sigma_0 , \tag{1}$$

$$\frac{\sigma_M}{\sigma_0} = \left(1 + \frac{E\varepsilon_M^p}{\sigma_0}\right)^n \quad \text{when } \sigma_M > \sigma_0 , \tag{2}$$

where the subscripts (i) (see Table 1) are omitted for clarity.

In the present paper the aim is to establish which mode dominates as a function of the yield stress mismatch. The yield stress of the grain interior is indeed the parameter that can most easily be modified experimentally by proper ageing treatment. Such a quantitative analysis of this highly non-linear problem of failure mode transition requires a detailed model for void growth and coalescence to be incorporated in both grain and grain boundary areas. Predictions of the model will be used to interpret some experimental findings on the failure modes of 7000 aluminium alloys whose microstructure have been varied in a controlled manner through appropriate heat treatments [1,2].

Table 1. Definition of the geometrical and mechanical parameters of the constitutive model.

Geometric parameters	
$D_{(i)x}$ and $D_{(i)z}$	Mean transverse and longitudinal diameter of defects
$L_{(i)x}$ and $L_{(i)z}$	Mean transverse and longitudinal spacing between voids
h and d	PFZ thickness and half grain size
$R = h/(h+d)$	relative PFZ thickness
$f_{(i)} = \frac{1}{12}\frac{D_{(i)x}^2 D_{(i)z}}{L_{(i)x}^2 L_{(i)z}}$	Void volume fraction (in the PFZ, $L_{pz}=h$)
$W_{(i)} = \frac{D_{(i)z}}{D_{(i)x}}$	Void aspect ratio
$\lambda_{(i)} = \frac{L_{(i)z}}{L_{(i)x}}$	Void distribution factor (in the PFZ, $L_{pz}=h$)
Mechanical parameters	
E	Young's modulus
ν	Poisson ratio
$\sigma_{0(i)}$	Yield stress
$n_{(i)}$	Strain-hardening exponent

2. Constitutive model for ductile damage

The material model used here is an elastic-viscoplastic continuum model for the growth and coalescence of spheroidal voids. The model will be used for both the PFZ and the grain interior, only accounting for a difference in mechanical properties and microstructure as shown in Fig. 1c.

The void growth stage

Pardoen and Hutchinson [4] have worked on a Gurson-type void growth model [5] that describes the plastic flow in a continuous porous medium. The model extends the contribution of Gologanu-Leblond-Devaux [6] to strain hardening. It is a full constitutive model for a porous elastoplastic material containing spheroidal voids. The model contains nine state variables: the six components of the mesoscopic stress tensor $\boldsymbol{\sigma}$, the porosity f; the void aspect ratio S, and the average yield stress of the matrix material σ_M. The void aspect ratio is defined by $S=\ln(W)$. For details the reader is referred to [4].

The equations of the void growth model are :

$$\Phi = \frac{C}{\sigma_M^2}\left\|\mathbf{s}+\eta\sigma_{hg}\mathbf{X}\right\| + 2q(g+1)(g+f)\cosh\left(\kappa\frac{\sigma_{hg}}{\sigma_M}\right) - (g+1)^2 - q^2(g+f)^2 \equiv 0 \quad (3)$$

$$\dot{f} = (1-f)tr\left(\dot{\boldsymbol{\eta}}^{\mathbf{p}}\right) \quad , \quad (4)$$

$$\dot{S} = \frac{3}{2}(1+h_1)\left(\dot{\boldsymbol{\eta}}^{\mathbf{p}} - \frac{1}{3}tr\left(\dot{\boldsymbol{\eta}}^{\mathbf{p}}\right)\underline{\underline{\mathbf{I}}}\right) : (\hat{\mathbf{e}}_{\mathbf{Z}} \otimes \hat{\mathbf{e}}_{\mathbf{Z}}) + h_2 tr\left(\dot{\boldsymbol{\eta}}^{\mathbf{p}}\right) \quad , \quad (5)$$

$$\sigma_M \dot{\varepsilon}_M^p (1-f) = \boldsymbol{\sigma} : \dot{\boldsymbol{\eta}}^{\mathbf{p}} \quad , \quad (6)$$

$$\dot{\boldsymbol{\eta}}^{\mathbf{p}} = \Lambda\frac{\partial\Phi}{\partial\boldsymbol{\sigma}} \quad , \quad (7)$$

$$\dot{\varepsilon}_M^p = \dot{\varepsilon}_0\left[\frac{\sigma_M}{g_1\left(\varepsilon_M^p\right)}\right]^{\frac{1}{m}} \quad . \quad (8)$$

where Φ is the flow potential; $\dot{\boldsymbol{\eta}}^{\mathbf{p}}$ is the mesoscopic plastic strain tensor; eqs (4) and (5) are the evolution laws for f and S, respectively, with $\boldsymbol{s}$ the deviatoric stress tensor, σ_{hg} a generalized hydrostatic stress, and $\boldsymbol{X}$ a tensor defined by $\frac{2}{3}\hat{\mathbf{e}}_{\mathbf{Z}} \otimes \hat{\mathbf{e}}_{\mathbf{Z}} - \frac{1}{3}\hat{\mathbf{e}}_X \otimes \hat{\mathbf{e}}_X - \frac{1}{3}\hat{\mathbf{e}}_Y \otimes \hat{\mathbf{e}}_Y$, where $\{\hat{\mathbf{e}}_{\mathbf{X}}, \hat{\mathbf{e}}_Y, \hat{\mathbf{e}}_Z\}$ is an orthonormal basis with $\hat{\mathbf{e}}_{\mathbf{Z}}$ parallel to the cavity axis; the rotation of the cavity is assumed to follow the rotation of the material axis.

Strain rate sensitivity is included in the model by taking the response of the matrix material to be elastic-viscoplastic. The matrix material is assumed to deform by power law relation in addition to elasticity. The plastic part of the Lagrangian strain rate is given by (8), with m being the strain rate hardening exponent, and $\dot{\varepsilon}_0$ the reference strain rate. The function $g_1(\varepsilon_M^p)$ in (8) represents the effective tensile flow stress in the matrix material in a tensile test carried out at a strain rate $\dot{\varepsilon}_M^p = \dot{\varepsilon}_0$. Thus for a power hardening material with uniaxial stress strain behaviour, the function $g_1(\varepsilon_M^p)$ is given by (2). The details of the expressions relating the parameters appearing in eq (3) to (5) (e.g. C, η, q, g, κ, B, D, h_1, h_2) to the state variables of the model are provided in [4].

Void coalescence

The coalescence model, derived from Thomason's criterion for the onset of coalescence [7], directly addresses the mechanism of tensile plastic localization in the ligaments between neighbouring voids, leading to a uniaxial mode of straining. The criterion of Thomason has been extended to strain-hardening materials in [4]. In order to couple the coalescence model with the void growth model (2) to (8), a new state variable related to the void distribution, $\chi = R_X / L_X$ (where R is the void radius), has been introduced.

Coalescence occurs when the stress component in the direction of the void axis reaches a critical value:

$$\sigma_n \equiv \boldsymbol{\sigma} : \left(\hat{\mathbf{e}}_{\mathbf{Z}} \otimes \hat{\mathbf{e}}_{\mathbf{Z}}\right) = \left(1-\chi^2\right)\left[\alpha\left(\frac{1-\chi}{\chi W^2}\right)^2 + \beta\sqrt{\frac{1}{\chi}}\right], \tag{9}$$

where the parameter α is given by the fit (for $0 \le n \le 0.3$) $\alpha = 0.1 + 0.217n + 4.83n^2$, while β can be considered as constant and equal to 1.24.

Once the criterion (9) is met, further straining develops uniaxially in the direction of the void axis:

$$\dot{\boldsymbol{\eta}}^C = \dot{\varepsilon}_n^C \ \left(\hat{\mathbf{e}}_{\mathbf{Z}} \otimes \hat{\mathbf{e}}_{\mathbf{Z}}\right), \tag{10}$$

where the normal strain rate is given by a power law relation similar to (8) :

$$\dot{\varepsilon}_n^p = \dot{\varepsilon}_0\left[\frac{\sigma_n}{g_2\left(\varepsilon_n^p\right)}\right]^{\frac{1}{m}} \tag{11}$$

But now $g_2(\varepsilon_n^p)$ is a softening relation assumed to be linear in ε_n^p, which is consistent with FE void cell calculation results (see [4] and [8]). The unloading slope depends mainly on the stress triaxiality, the void shape and the relative position of neighbouring voids. The values given for the unloading slope are motivated from finite element void cell calculations. Note that a precise determination of the slope is especially important at large stress triaxiality. Indeed, under highly constrained conditions, the work spent during the coalescence stage can be significant, on the order of the work spent during void growth [4].

The total strain rate tensor $\dot{\boldsymbol{\eta}}$ is decomposed in an elastic part $\dot{\boldsymbol{\eta}}^E$ and a viscoplastic part $\dot{\boldsymbol{\eta}}^{VP}$. The elastic response is governed by the hypo-elastic relationship

$$\overset{\nabla}{\boldsymbol{\sigma}} = \mathbf{R} : \dot{\boldsymbol{\eta}}^{\mathbf{E}} = \mathbf{R} : \left(\dot{\boldsymbol{\eta}} - \dot{\boldsymbol{\eta}}^{\mathbf{P}}\right), \tag{12}$$

in terms of the Jaumann stress-rate $\overset{\nabla}{\boldsymbol{\sigma}} = \dot{\boldsymbol{\sigma}} - \mathbf{W}\cdot\boldsymbol{\sigma} + \boldsymbol{\sigma}\cdot\mathbf{W}$ ($\mathbf{W}$ is the skew symmetric part of the velocity gradient $\mathbf{L}$). The fourth-order modulus tensor $\mathbf{R}$ is expressed in the usual way in terms of Young's modulus E and Poisson's ratio ν. During void growth, the viscoplastic strain rate is determined by eq. (7), $\dot{\boldsymbol{\eta}}^{VP} = \dot{\boldsymbol{\eta}}^{\mathbf{p}}$. When the coalescence criterion (9) is met, further straining is described by eq. (10), $\dot{\boldsymbol{\eta}}^{VP} = \dot{\boldsymbol{\eta}}^C$.

3. Finite element results

The constitutive model outlined in the previous section is analyzed using an incremental finite strain, finite element method. A plane strain, total Lagrangian, convected coordinate formulation is used [9]. The stable step size in the incremental numerical procedure is significantly increased by using a forward gradient method [11] for the void growth as well as the void coalescence part.

We analyze an infinitely large polycrystalline aggregate consisting of hexagonal grains (see Fig. 1), from which a unit cell can be identified. The material is subjected to uniaxial tension in the vertical direction ($\Sigma_1 = 0$). Fig. 2 shows the finite element mesh used to

represent two grains and the boundary in between, accounting for the symmetry of the problem. Each quadrilateral element is built up of four constant strain triangles. To ensure symmetry of the unit-cell during loading the edges of the unit-cell are constrained to remain straight. This is achieved by using a Rayleigh-Ritz technique that controls the normal displacement rates, such that the stress ratio, Σ_1/Σ_2, remains zero. Since the calculations are in plane strain the stress triaxiality $T = \Sigma_h / \Sigma_e$ is equal to 0.57, initially.

The competition between hardening and void softening in the PFZ is primarily driven by the flow properties of the grain with respect to the flow properties of the PFZ. The deformation of the two material parts is described by the constitutive model presented in section 2. The microstructural and micromechanical parameters of the model have been summarised in Fig. 1. The parameters are given the following values for typical 7000 aluminium alloys [1] :

f_{g0}	n_g	W_{g0}	λ_{g0}	σ_{0g}/E	R_0
10^{-3}	0.05	1	1	10^{-3}	0.1
f_{p0}	n_p	W_{p0}	λ_{p0}	L_{p0}/D_{p0}	$T=\Sigma_h/\Sigma_e$
$2.47\ 10^{-2}$	0.3	1	1	3	0.57

The key ingredients of the flow behaviour chosen are a PFZ softer than the grain interior, but presenting an enhanced work hardening rate [3]. The elastic constants are the same in both layers :

$\nu_g = \nu_p = \nu = 0.35$ and $E_g = E_p = E.$

The PFZ yield stress, specified through the ratio σ_{0g}/σ_{0p}, will take three distinct values: 4, 6 and 8. Fig. 3 presents the overall stress-strain curves for the three yield stress ratios. The sequence of fracture events is also shown through a chronological serie of numbers on the right hand side of Fig. 3.

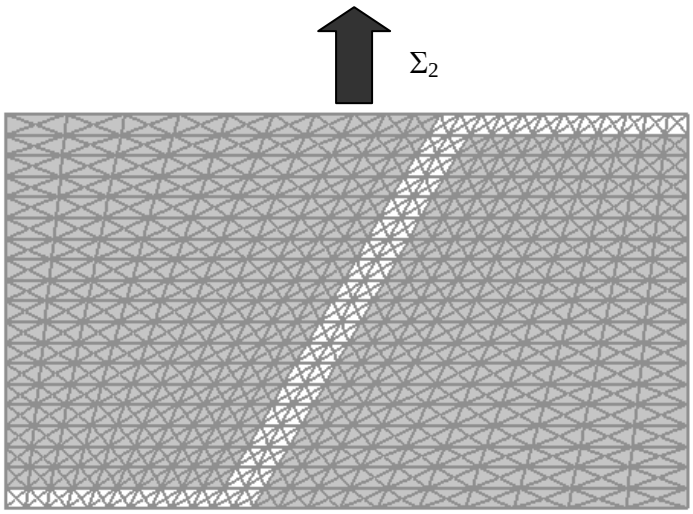

FIGURE 2. Finite element discretization of the unit-cell analysed.

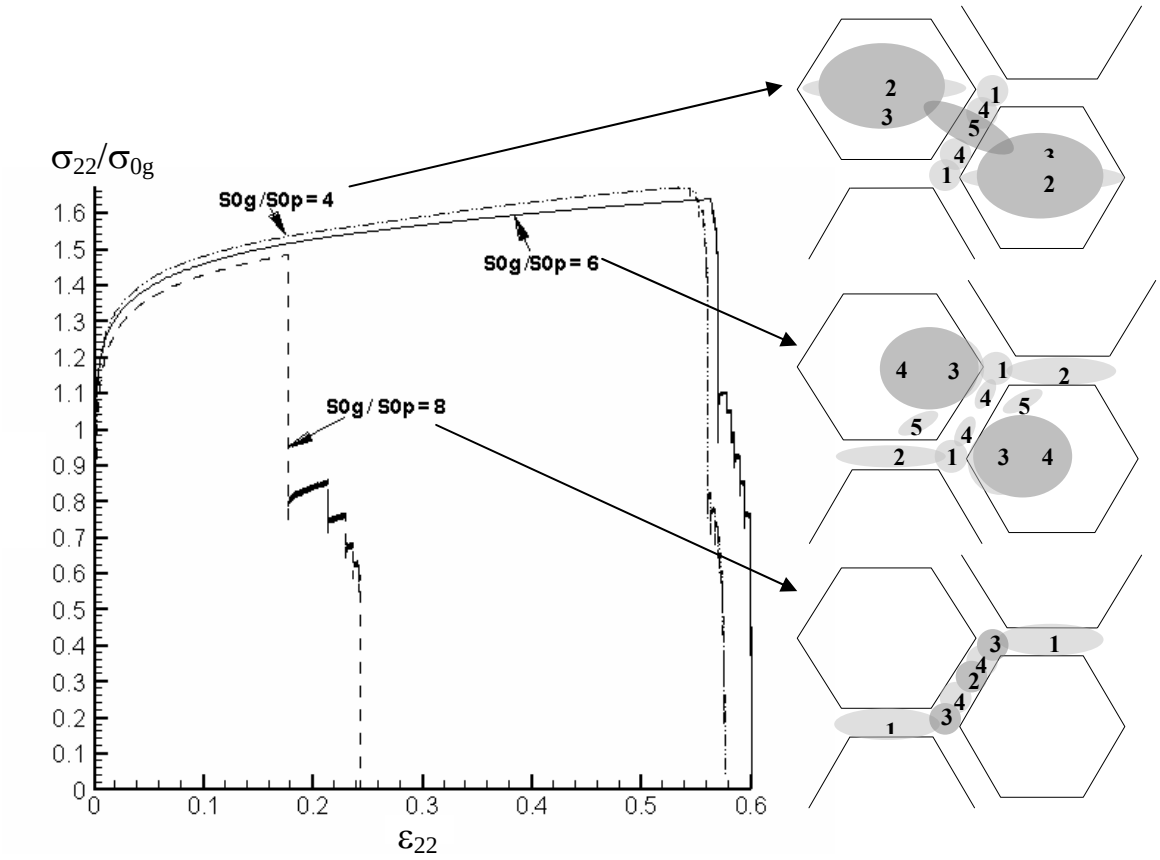

FIGURE 3. Macroscopic flow curves and corresponding cracks path for different values of the yield stress ratio between the grain and the PFZ.

The transition from intergranular to transgranular failure is captured. For a yield stress ratio equal to 8, the crack path is clearly intergranular. On the other hand, for a yield stress ratio equal to 4, failure is transgranular. The grain boundary fails only to join the cracked grains. A yield stress ratio equal to 6 gives an intermediate situation, where damage initiated at the triple grain junctions spreads at the same time in the grain and along the boundaries. So, as expected from [3], an increase of the grain yield stress promotes grain boundary failure. Indeed, the high sensitivity of the transition to an intergranular failure mode on the grain strength has been observed by many investigators in both tensile tests (low stress triaxiality) and fracture tests (high stress triaxiality), e.g. [2].

Note that the intergranular contribution for σ_{0g}/σ_{0p}= 6, which is mostly controlled by transgranular failure. The saw-tooth shape of the stress-strain curve during the coalescence phase shows that the microstructure is fractured progressively during deformation. This is a consequence of the size of the unit cell being too small to capture adequately the average behaviour of a random polycrystalline material. A larger unit-cell with random grains is necessary to reproduce a more realistic polycrystalline response.

4. Conclusion and perspectives

A multiscale model featuring a soft and a hard damaging zone has been developed in order to elucidate the competition between grain boundary and transgranular failure in aluminium alloys. As a first prediction, a higher grain yield stress increases the risk of grain boundary

failure within the precipitate free zone (PFZ), which is consistent with experimental measurements performed on 7040 and 7050 alloys [2].

A more systematic investigation of the inter/transgranular competition is planned in order to elucidate the influence of the other mechanical and microstructural parameters on the ductility and the selected failure mode; the results will be presented in the form of "failure mechanism maps" showing ductility versus stress triaxiality. Furthermore, the model permits to study crack propagation for a large range of stress triaxialities, including stress triaxialities of 3-4 present in a sharp crack tip process zone. In particular, the effect of the relative void spacing and hardening capacity on the ductility will be investigated.

Acknowledgements – The support of the Walloon Region (DGTRE) and the Fonds Social Européen through a "FIRST EUROPE Objectif 3" project is gratefully acknowledged. This research is also carried out under the interuniversity attraction poles P5/08, funded by the Belgian Science Policy.

References

1. Dumont, D., *Relations Microstructure/Ténacité dans les Alliages Aéronautiques de la Série 7000*, Ph.D. Thesis, Institut National Polytechnique de Grenoble, 2001.
2. Dumont, D., Deschamps, A. and Brechet, Y., *Materials Science and Engineering*, Vol. 356, 326-336, 2003.
3. Pardoen, T. *et al.*, *Journal of the Mechanics and Physics of Solids*, Vol. 51, 637-665, 2003.
4. Pardoen, T. and Hutchinson, J.W., *Journal of the Mechanics and Physics of Solids*, Vol. 48, 2467-2512, 2000.
5. Gurson, A.L., *Journal of Engineering Materials and Technology*, Vol. 99, 2-15, 1977.
6. Gologanu, M. *et al.*, In *Suquet, P. (Ed.) Continuum Micromechanics*, Springer-Verlag, 1995.
7. Thomason, P.F., *Ductile Fracture of Metals*, Pergamon Press, Oxford, 1990.
8. Tvergaard, V., *Computational Mechanics*, Vol. 20, 186-191, 1997.
9. Tvergaard, V., *Advances in applied Mechanics*, Vol. 27, 83-151, 1990.
10. Onck, P.R. and Van der Giessen, E., *Journal of the Mechanics and Physics of Solids*, Vol. 47, 99-139, 1999.
11. Pierce, D. *et al.*, *Computers and Structures*, Vol.18, 875-887, 1984.